Motility-induced phase separation and frustration in active matter swarmalators

B. Adorjáni,[1] A. Libál,[1] C. Reichhardt,[2] and C. J. O. Reichhardt[2]
[1]*Mathematics and Computer Science Department, Babeş-Bolyai University, Cluj 400084, Romania*
[2]*Theoretical Division and Center for Nonlinear Studies, Los Alamos National Laboratory, Los Alamos, New Mexico 87545, USA*

(Received 26 September 2023; accepted 9 January 2024; published 26 February 2024)

We introduce a two dimensional system of active matter swarmalators composed of elastically interacting run-and-tumble active disks with an internal parameter ϕ_i. The disks experience an additional attractive or repulsive force with neighboring disks depending upon their relative difference in ϕ_i, making them similar to swarmalators used in robotic systems. In the absence of the internal parameter, the system forms a motility-induced phase separated (MIPS) state, but when the swarmalator interactions are present, a wide variety of other active phases appear depending upon whether the interaction is attractive or repulsive and whether the particles act to synchronize or ant-synchronize their internal parameter values. These phases include a gas-free gel regime, arrested clusters, a labyrinthine state, a regular MIPS state, a frustrated MIPS state for attractive antisynchronization, and a superlattice MIPS state for attractive synchronization.

DOI: 10.1103/PhysRevE.109.024607

I. INTRODUCTION

Active matter systems contain self-motile particles and can be found in soft matter [1–3], biological [4–8], social [9,10], active topological [11,12], and robotic [13–15] contexts. These active matter systems are challenging to model, and have an interesting collective behavior, as the motor forces inject energy into the system locally, meaning that active matter systems are out of equilibrium and present a lack of detailed balance and of time-reversal symmetry. This opens up the possibility of emergent collective behaviors, such as collective motion to escape a region with multiple obstacles present or, in case of bacteria, to more optimally search for food. This makes active matter systems prime candidates to form so called intelligent materials—systems adaptable to multiple functions, highly responsive to external stimuli, and able to perform tasks in response to these external stimuli. Such systems are widespread in biology, two examples of them being the bacterial colonies and the biological tissues. It is also possible to mimic these complex behaviors in artificial active matter systems and assemblies of robotic systems that could move and perform tasks together as a swarm [16–19]. The simplest models of active matter consist of interacting elastic disks undergoing a run-and-tumble motion or driven Brownian diffusion. Even in the absence of any attractive forces, such motion produces what is known as motility-induced phase separation (MIPS) when the activity level and the disk density are sufficiently large [19–27]. For monodisperse particles, the dense clusters in the MIPS state have triangular order and coexist with a lower density gas. An open question is whether there can be other types of MIPS regimes that have alternative ordering within the clusters. Also unknown is whether inclusion of more complex particle-particle interactions can lead to a comprehensive way to connect different MIPS regimes within one model.

In many soft and condensed matter systems that have competing or multilength scale interactions, additional larger scale patterning can arise [28–33]. Frustration effects can occur when not all of the constraints in the system can be satisfied simultaneously, as is the case for proton ordering in water ice [34], frustrated colloidal systems [35,36], spin ice [37], artificial spin ice systems [38,39], and certain types of metamaterials [40]. There are potentially many active systems where additional competing interactions could be added that would create additional regimes or frustration effects that might interfere with the crystalline ordering in the dense phase of MIPS.

Here we consider a model of run-and-tumble active disks that exhibit a MIPS phase for sufficiently high activity and density. We give each disk an internal parameter ϕ_i and introduce an additional attractive or repulsive force between neighboring disks i and j based on the swarmalator rules for internal parameter differences $\delta\phi_{ij}$ [41]. This internal parameter evolves as a function of time and also changes due to interactions with neighboring disks located within a radius $2r_{\rm sw}$. A schematic illustration of the model appears in Fig. 1. The parameter J controls the strength and sign of the translational force exerted along the line connecting two disks i and j depending on the magnitude of $\delta\phi_{ij}$. A second parameter K determines how rapidly the value of ϕ_i changes in response to $\delta\phi_{ij}$, with positive values of K resulting in a net reduction of $\delta\phi_{ij}$ and negative K values causing $\delta\phi_{ij}$ to increase. With these additional interactions, we find that a wide variety of active matter regimes can be realized, including distinctive MIPS states that revert back to the ordinary MIPS state in the limit $J = 0$, $K = 0$. For $J > 0$, the MIPS state contains a hexagonal superlattice structure of disks with similar internal parameter values surrounded by a gas of misaligned disks. We also observe a gel state at $K = 0$, where the internal parameter can take on multiple values as it is not synchronized, and a frustrated liquid at high K values where the superlattice is

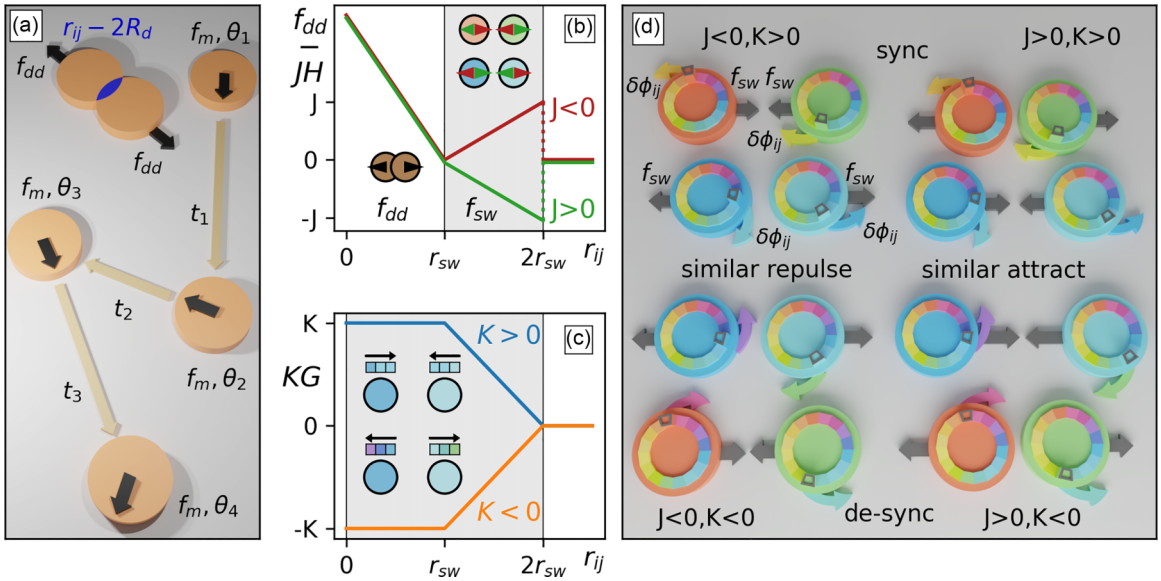

FIG. 1. (a) Colliding disks experience a steric repulsion force $f_{\rm dd}$. Each disk also undergoes run-and-tumble motion with a motor force of $f_{\rm m}$ pointing in a direction set by the angle θ_i for a time t_i, with new random values of θ_i and t_i selected during each instantaneous tumbling event. (b) $f_{\rm dd} - JH$, the disk-disk forces, and the function $-JH(r_{ij})$ vs the distance r_{ij} between disks. Only steric disk repulsion acts when $r_{ij} \leqslant r_{sw}$. The value of $JH(r_{ij})$ becomes nonzero when $r_{sw} < r_{ij} \leqslant 2r_{sw}$; it is negative when $J > 0$ (green) and positive when $J < 0$ (red). The left inset shows the steric interactions (brown disks). The upper center inset shows swarmalator interactions between disks with internal parameters that differ more than $\pi/2$, which is repulsive for $J > 0$ (green arrows) and attractive for $J < 0$ (red arrows). The lower center inset shows the swarmalator interactions when the disks have internal parameters that differ less than $\pi/2$, which is attractive for $J > 0$ (green arrows) and repulsive for $J < 0$ (red arrows). (c) The function $KG(r_{ij})$ controlling the evolution of the internal parameter. When $K > 0$ (blue), the internal parameter of neighboring disks becomes synchronized over time, as illustrated by the boxes in the top inset that show how the phase changes as a function of time. When $K < 0$ (orange), the internal parameters become desynchronized over time, as shown by the boxes in the lower inset. (d) Summary of swarmalator forces for the four possible nonzero combinations of J and K. Disk color indicates the value of the internal parameter, and the possible values of this parameter appear as a ring inside each disk. Gray arrows show the orientation of $f_{\rm sw}$ for each combination, while the curved colored arrows indicate the direction in which the internal parameter will evolve as a result of the interaction. For each combination, we show a pair of disks where the internal parameter difference is smaller than $\pi/2$ (blue colored disks), and a pair where the difference is larger than $\pi/2$ (green and orange disks).

unable to form. We map the evolution of these distinct states as a function of activity and density and find that MIPS is enhanced for the combination $K < 0$ and $J > 0$, but is suppressed for other combinations.

Our model could be realized using robotic swarms with steric interactions and swarmalator rules [42,43]. The term "swarmalator" was originally introduced in these robotic swarm systems, where it denotes an interaction among the robots based on their internal state, and served as an inspiration for our active matter system with the additional interaction, also based on an internal state that is not coupled to the other parameters of the active motion.

In addition to robotic systems, such interactions that depend on the internal state of the individual particles could arise for biological systems of motile cells of different types in which individual cells are attracted to one cell type but repelled by a different cell type [44]. There are also a variety of soft matter systems that can have particle-specific or competing attractive and repulsive interactions with each other, or that have multiple length scales in their interactions, which can create pattern forming states [28–30,33,45,46]. It should also be feasible to create competing interactions using light activated colloids with feedback loops [47–49].

II. MODEL

We consider a two-dimensional system of size $S_x = 160$ and $S_y = 160$ with periodic boundary conditions in the x and y directions, containing $N = 4000$ circular disks of radius of $R_d = 1.0$. The disk density is given by $\rho = N\pi R_d^2/(S_x S_y)$. As shown in Fig. 1(a), disk i interacts sterically at short range with other disks according to $\mathbf{f}_{\rm dd} = f_{\rm dd}\hat{\mathbf{r}}_{ij}$ with $f_{\rm dd} = \sum_j^N k(2R_d - r_{ij})\Theta(2R_d - r_{ij})$, where $r_{ij} = |\mathbf{r}_j - \mathbf{r}_i|$ is the distance between the centers of disks i and j, $\hat{\mathbf{r}}_{ij} = (\mathbf{r}_j - \mathbf{r}_i)/r_{ij}$, Θ is the Heaviside step function, and $k = 20.0$ is the elastic constant. Run-and-tumble motion is produced by a motor force $\mathbf{f}_m$ of magnitude $f_m = 1$, where the angle $\theta_i \in [0, 2\pi)$ sets the direction that the motor force is applied in for a duration of $t_i \in [\tau, 2\tau]$. At the end of each running event, an instantaneous tumbling event occurs in which new values of θ_i and t_i are chosen randomly from the allowed intervals with uniform distributions.

Each particle is endowed with an internal parameter $\phi_i \in [0, 2\pi)$ that is not coupled to θ_i. The internal parameter undergoes a slow thermal diffusion that is independent of the surroundings of the disk. The thermal force F_i^T is implemented using Langevin kicks with the properties $\langle F_i^T \rangle = 0$ and $\langle F_i^T(t) F_i^T(t') \rangle = 2k_B T \delta_{ij} \delta(t - t')$. Here we use a small

thermal force magnitude of $F^T = 0.001$. The value of ϕ_i is also modified by a forcing term of strength K that is dependent on the difference between the internal parameters $\delta\phi_{ij} = (\phi_j - \phi_i)$ of neighboring disks within a radius of $r_{ij} \leqslant 2r_{\rm sw}$ where $r_{\rm sw} = 2R_d$. This gives

$$\frac{d\phi_i}{dt} = \sum_j^N K \sin(\delta\phi_{ij}) G(r_{ij}) + F_i^T, \tag{1}$$

where $G(r_{ij}) = 1$ for $r_{ij} \leqslant r_{\rm sw}$, $G(r_{ij}) = (2r_{\rm sw} - r_{ij})/r_{\rm sw}$ for $r_{\rm sw} < r_{ij} \leqslant 2r_{\rm sw}$, and $G(r_{ij}) = 0$ for $r_{ij} > 2r_{\rm sw}$. The form of $G(r_{ij})$ is illustrated in Fig. 1(c). When $K > 0$, the internal parameters of neighboring disks tend to become synchronized, while when $K < 0$, the internal parameters tend to become antisynchronized.

The positions of the disk centers are obtained by integrating the following equation of motion:

$$\eta \frac{d\mathbf{r}_i}{dt} = \mathbf{f}_{\rm m} + \mathbf{f}_{\rm dd} + \mathbf{f}_{\rm sw}, \tag{2}$$

where we set the damping coefficient to $\eta = 1$. This is the parameter that connects the units of the force, distance, and time in our simulation, and it can be used to rescale these units to match experimental values. The swarmalator interaction force is given by $\mathbf{f}_{\rm sw} = f_{\rm sw}\hat{\mathbf{r}}_{ij}$ with

$$f_{\rm sw} = -\sum_j^N J \cos(\delta\phi_{ij}) H(r_{ij}), \tag{3}$$

where $H(r_{ij}) = 0$ for $r_{ij} \leqslant r_{\rm sw}$, or $r_{ij} > 2r_{\rm sw}$ and $H(r_{ij}) = (r_{ij} - r_{\rm sw})/r_{\rm sw}$ for $r_{\rm sw} < r_{ij} \leqslant 2r_{\rm sw}$. As shown in Fig. 1(b), disks with similar internal parameters repel each other when $J < 0$ and attract each other when $J > 0$. When $J = 0$, the internal parameter has no impact on the disk dynamics and the model reverts to the normal MIPS behavior found in the absence of swarmalator interactions. Figure 1(d) summarizes the four possible interaction regimes for nonzero combinations of J and K.

We numerically integrate Eqs. (1) and (2) using a simulation time step of $dt = 0.001$. To initialize the sample, we place all disks in randomly chosen nonoverlapping positions and set the initial values of θ_i, ϕ_i, and t_i to random values chosen from the allowed range of each quantity. We allow the system to evolve for 2×10^6 simulation time steps before collecting data during the next 3×10^6 simulation time steps.

III. RESULTS

In Fig. 2, we plot a dynamic phase diagram for samples with $\rho = 0.49$ and $\tau = 1.5 \times 10^5$ as a function of K versus J, where we highlight the seven regimes of behavior. For this choice of τ, an isolated disk undergoing no collisions would travel a distance $d_{\rm free}$ ranging from $d_{\rm free} = 150$ to $d_{\rm free} = 300$, comparable to the system size. When $K = 0$ and $J = 0$ the system forms an ordinary MIPS state, which we designate as region II. This MIPS phase extends along the $J = 0$ axis for all values of K, since the swarmalator interaction has no effect on the disk motion when $J = 0$. The MIPS state persists for small values of $|J|$ when the swarmalator force remains too small to perturb the motion significantly. In region I, where $J > 0$ and $K > 0$, all of the disks evolve to have the same internal parameter $\phi_{\rm bulk}$, the swarmalator force becomes attractive, and a gas-free gel state emerges, as illustrated in Fig. 3(a).

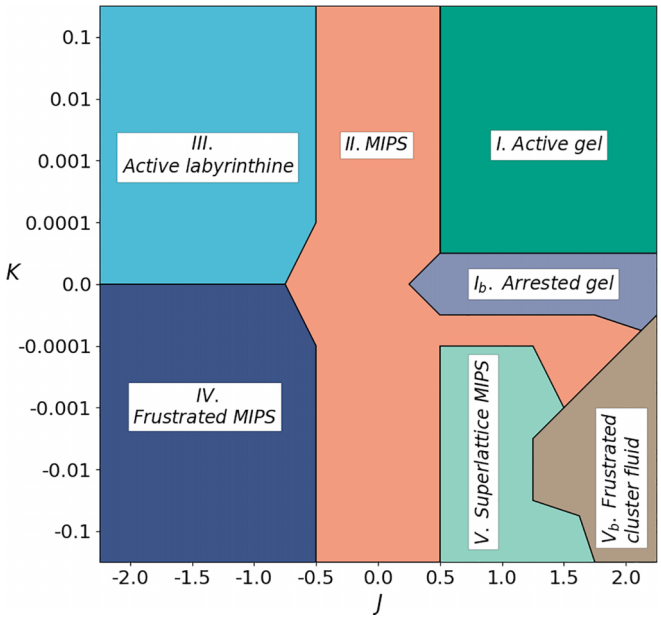

FIG. 2. Dynamic phase diagram as a function of K, the synchronization factor, and J, the swarmalator force strength, for an active disk system with a density of $\rho = 0.49$ at $\tau = 1.5 \times 10^5$. Region I with $K > 0$ and $J > 0$ is the active gel where all of the disks synchronize to the same internal parameter, as shown in Fig. 3(a). Region II is the ordinary MIPS phase for $J = 0$, illustrated in Fig. 4(d). Region III for $J < 0$ and $K > 0$ is the active labyrinthine state shown in Fig. 3(b) where the disks synchronize to the same internal parameter. In region IV for $K < 0$ and $J < 0$ we find the frustrated MIPS phase illustrated in Figs. 3(c) and 4(a) with stripe ordering in the clusters, while region V for $K < 0$ and $J > 0$ is a superlattice MIPS phase as shown in Figs. 3(d) and 4(b). Region I_b is the arrested gel phase shown in Figs. 5(a) and 5(c), and region V_b is a frustrated cluster fluid, illustrated in Figs. 5(b) and 5(d).

We find the same gel state for most choices of τ and ρ, but as τ increases, the gel forms more rapidly. The value of $\phi_{\rm bulk}$ differs depending on the initial conditions, as particles that are closer together initially are synchronizing faster toward each other in their internal parameter, and eventually all of the disks always reach $\phi_i = \phi_{\rm bulk}$ after a transient time that becomes longer as K becomes smaller. At $K = 0$, for all positive J we find region I_b, where there is no global ordering of ϕ_i. Instead, small, gellike clusters form with a coherent internal parameter and with no surrounding free gas state, as shown in Figs. 5(a) and 5(c). In both regions I and I_b, the gel clusters slowly drift through the system as a result of the disk activity.

For $K > 0$ and $J < 0$ in Fig. 2, we find region III where the disks synchronize to a single global internal parameter value $\phi_{\rm bulk}$ but repel each other. Here a labyrinthine pattern appears, as illustrated in Fig. 3(b). Due to the activity, region III has some characteristics of a fluctuating fluid. The disks do not form a crystal because the repulsive swarmalator force drops to zero when the particles touch ($r_{ij} = 2R_d$) and is maximal when $r_{ij} = 4R_d$. The labyrinthine structures are similar to the labyrinthine and cluster phases found in systems with multiple

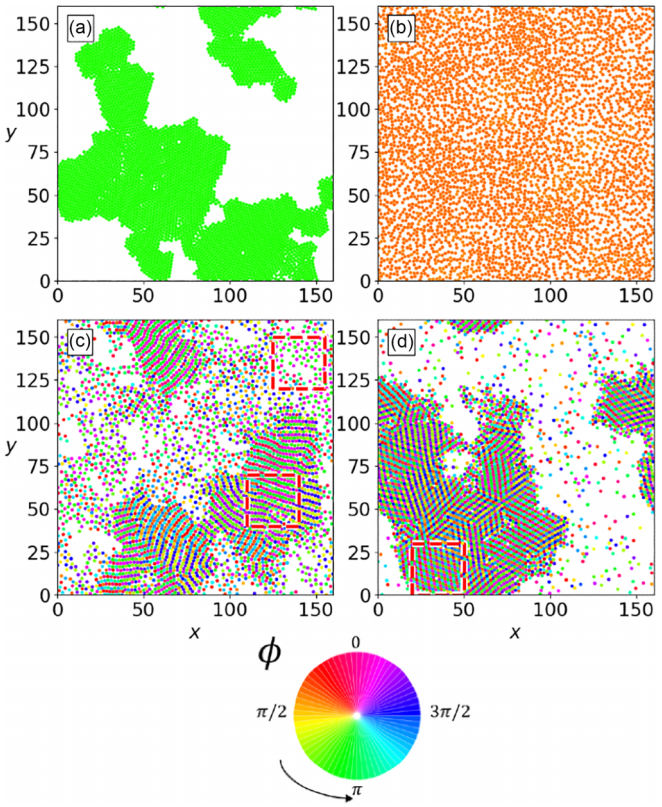

FIG. 3. Illustrations of the disk locations (circles) and internal parameters (indicated by color) for the dynamic phases described in Fig. 2 in a system with $\rho = 0.49$ and $\tau = 1.5 \times 10^5$. (a) Region I, the gel state where all disks have the same value of ϕ_i, at $J = 1.0$ and $K = 0.1$. (b) Region III, the fluid labyrinthine state where all disks have the same value of ϕ_i, at $J = -1$ and $K = 0.001$. (c) Region IV, the frustrated MIPS state with stripe ordering of ϕ_i inside the clusters, at $J = -1.5$ and $K = -0.1$. (d) Region V, the superlattice MIPS state, at $J = 1.0$ and $K = -0.1$. We show the color code for the different internal parameters separately under the panels. Videos of these phases are available in the Supplemental Material [50].

length scale repulsive potentials [29,45]. In our case, there is a core repulsive force from the elastic repulsion extending out to $r_{ij} = 2R_d$ that is surrounded by a softer intermediate range swarmalator repulsive force from $2R_d < r_{ij} \leqslant 4R_d$. In nonactive systems where this type of two-step repulsion is present, a range of additional crystalline and stripelike phases appear for varied densities [29,30]; however, the activity in our system prevents the formation of such higher-order structures.

For $K < 0$ and $J < 0$ we observe a frustrated MIPS state that we denote region IV in Fig. 2. This consists of a high-density solid with stripelike ordering of the internal parameter, coexisting with a fluid that contains locally ordered patches, as shown in Fig. 3(c). A blow up in Fig. 4(a) of one of the dense regions indicates that disks with a given value of ϕ_i form stripes that are interleaved between disks with the opposite internal parameter. A considerable number of lattice defects are present in the dense patches and the internal parameters are continuously changing due to the activity. Within region IV, the disks are attempting to antisynchronize their internal parameter with the parameters of the neighboring particles.

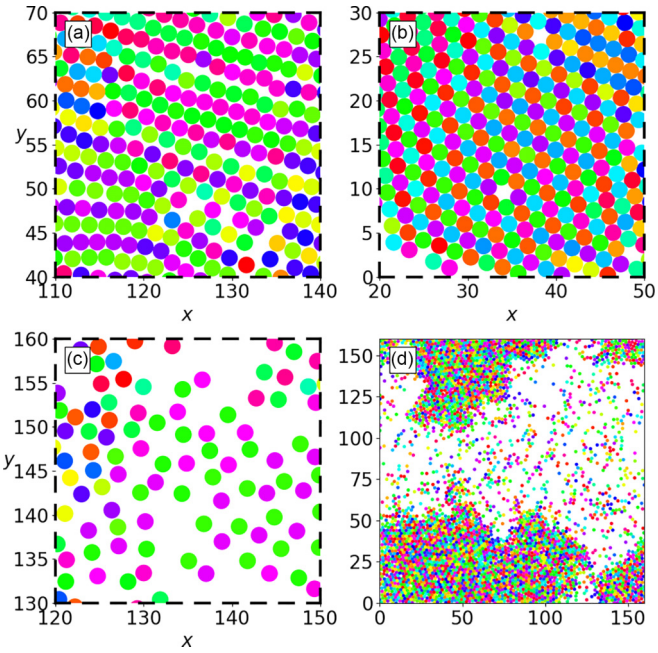

FIG. 4. (a) A blowup of the lower red dashed box in Fig. 3(c) showing stripe ordering in the dense portion of the frustrated MIPS state. (b) A blowup of the red dashed box in Fig. 3(d) showing a detail of the superlattice ordering in the superlattice MIPS state. (c) A blowup of the upper red dashed box in Fig. 3(c) showing the fluid portion of the frustrated MIPS state where the internal parameters are correlated. (d) Region II, the MIPS state, with no ordering of the internal parameter at $J = 0$ and $K = 0$.

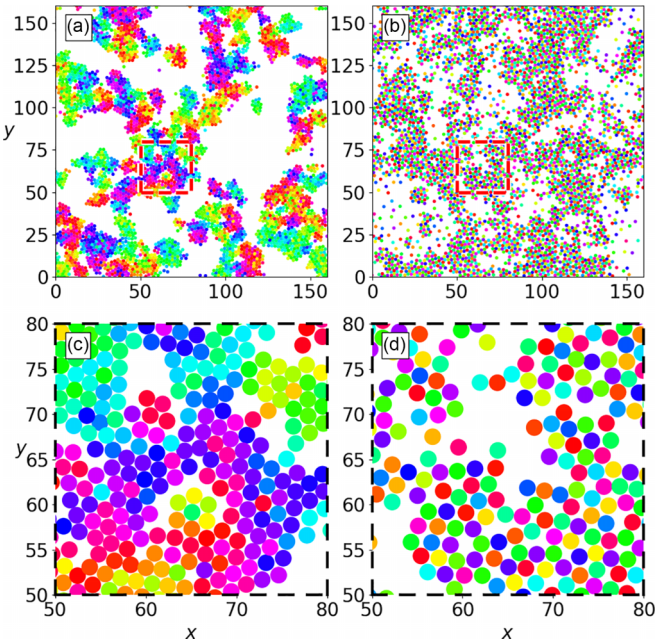

FIG. 5. (a) Region I_b or the arrested gel state at $J = 1.5$ and $K = 0$, where the system separates into clusters with the same internal parameter, but cannot fully coarsen due to the repulsive interactions between disks with opposite internal parameters. (b) Region V_b, the fluctuating clump state with local antisynchronized internal parameter ordering, at $J = 1.5$ and $K = -0.01$. (c) A blowup of the red dashed box for region I_b in panel (a). (d) A blowup of the red dashed box for region V_b in panel (b).

Once this antisynchronization is successful, the disk is attracted to its neighbors, but disks with the same value of ϕ_i repel each other. Formation of the striped order in the internal parameter is favored, because this allows each disk to maximize the number of nearest neighbors with attractive interactions while minimizing the number of neighbors with repulsive interactions. The internal parameter ordering pattern resembles the patterns found for frustrated spins on a hexagonal lattice or the buckling of colloidal particles that have been packed into slightly more than a monolayer [35,51,52]. In the case of the colloidal system, the colloidal particles are a little too dense to form a triangular solid, but can maintain their triangular arrangement by buckling out of plane, giving each particle an effective spin degree of freedom and permitting the system to form an antiferromagnetic Ising-like state that is frustrated on a hexagonal lattice. The frustrated state breaks up into multiple stripelike domains that each have different orientations of the buckled pattern.

Although region IV is related to a MIPS state, it has a larger number of disks in the gas state compared to ordinary MIPS and these disks exhibit a local internal parameter ordering, as illustrated in Fig. 4(c). The gas phase particles form loose pairs that have opposite values of ϕ_i. This ordering occurs only very locally and the specific values of ϕ_i for the opposing pairs vary from one gaseous patch to the next. Although this locally ordered liquid structure is preferred by the system at low densities, it is susceptible to the shear and compression produced by the activity of the disks, so it does not remain stable as a function of time but forms and disintegrates constantly in order to establish a dynamical equilibrium with the dense striped crystalline patches.

For $J > 0$ and $K < 0$, the system forms a more stable superlattice MIPS state, termed region V, where the dense regions develop a hexagonal superlattice ordering, illustrated in Fig. 3(d). For these parameters, disks with the same internal parameters attract each other and disks with the opposite internal parameters repel each other, but the internal parameters of neighboring disks evolve to be different from each other. To minimize the competition between attractive and repulsive interactions, the system forms the dense hexagonal superlattice ordering shown in more detail in Fig. 4(b). The swarmalator force decreases as r_{ij} decreases and vanishes when $r_{ij} = 2R_d$, so disks that are in direct contact can avoid being repelled by each other. Locally the system then can be described as repulsively interacting particles on a triangular lattice with a large lattice constant, and the superlattice ordering emerges from the desynchronization of the internal parameters of neighboring particles.

In Fig. 4(d), we show the regular MIPS state or region II at $K = 0$ and $J = 0$, where the disks maintain the same random internal parameters they received during initialization; however, since the internal phases play no role in the dynamics, the dense region develops with no internal parameter ordering. The regular MIPS state extends along the K axis for a band of finite width in J, since when J is sufficiently weak, the evolution of the internal parameter does not change the disk dynamics. We also find a window of region II for larger positive J and small but finite negative K; here, the antisynchronization is not strong enough to alter the internal phases and produce region V or V_b behavior.

In Fig. 5(a), we illustrate the configuration for what we call region I_b, or the phase arrested gel, which occurs for $K = 0$ and $J > 0$. In this case, the system starts with the disks assigned to random internal parameters, but since $K = 0$, these phases cannot evolve with time, so the system can be viewed as containing active particles that have randomized attractive and repulsive interactions with each other. Over time, the disks segregate into clumps of uniform internal parameters, but the formation of a single clump as in the gel state or region I is not possible because clumps with opposite internal parameters repel each other. A blow up of this state appears in Fig. 5(c). The frustrated clump fluid or region V_b that appears for $K < 0$ and $J > 1.5$ is illustrated in Fig. 5(b). The internal parameter configuration is not ordered within the solid clumps and the clusters are less compact and show larger fluctuations than the region II regular MIPS state. Although there is no superlattice ordering within the cluster, particles with the same internal parameter generally try not to be next to each other. This region appears when J becomes large enough that the repulsive and attractive forces destabilize the solid that forms in region V.

The different regimes can be distinguished using several measures. The circularly averaged internal parameter is given by

$$\bar{\phi} = \arctan2\left(\frac{1}{N}\sum_{i=1}^{N}\sin(\phi_i), \frac{1}{N}\sum_{i=1}^{N}\cos(\phi_i)\right). \tag{4}$$

This quantity is calculated every 5000 simulation time steps and we then compute the time average $\langle\bar{\phi}\rangle$ from $M = 600$ measurements. We obtain the standard deviation $\sigma = \sqrt{\sum_k^M(\bar{\phi}_k - \langle\bar{\phi}\rangle)^2/(M-1)}$, and plot a heat map of σ as a function of K versus J in Fig. 6(a). For $K > 0$, σ drops to zero since all of the internal parameters synchronize to a global value ϕ_{bulk}. For $K = 0$, σ takes on a small finite value since the small thermal fluctuations of the individual internal parameters are no longer suppressed by synchronization, while for $K < 0$, σ becomes large since the disks evolve to have internal parameters opposite from those of their neighbors.

We define the average frustration f as the sum,

$$f = \left\langle \frac{1}{N}\sum_{i=1}^{N} f_i \right\rangle, \tag{5}$$

of the individual disk frustration values f_i,

$$f_i = -\frac{1}{n}\text{sgn}(J)\text{sgn}(K)\sum_{j=1}^{N}\cos(\delta\phi_{ij})\Theta(4R_d - r_{ij}), \tag{6}$$

where the average is taken over time. An individual disk with no frustration has $f_i = -1$. Examples where frustration does not occur include disks in region II with $J = 0$ and $K = 0$, disks that have no neighbors within a radius $r_{ij} = 4R_d$, or disks for which all of the neighbors satisfy both the J and K interactions such as in the gel state of region I. In Fig. 6(b) we plot a heat map of f, which ranges from $-1 \leqslant f \leqslant 1$, as a function of K versus J. We find $f = +1$ (maximum frustration) in region III where the internal parameters are aligned but the swarmalator interaction forces are repulsive. In the frustrated MIPS state of region IV, f is close to zero but negative, indicating intermediate frustration, while in region V

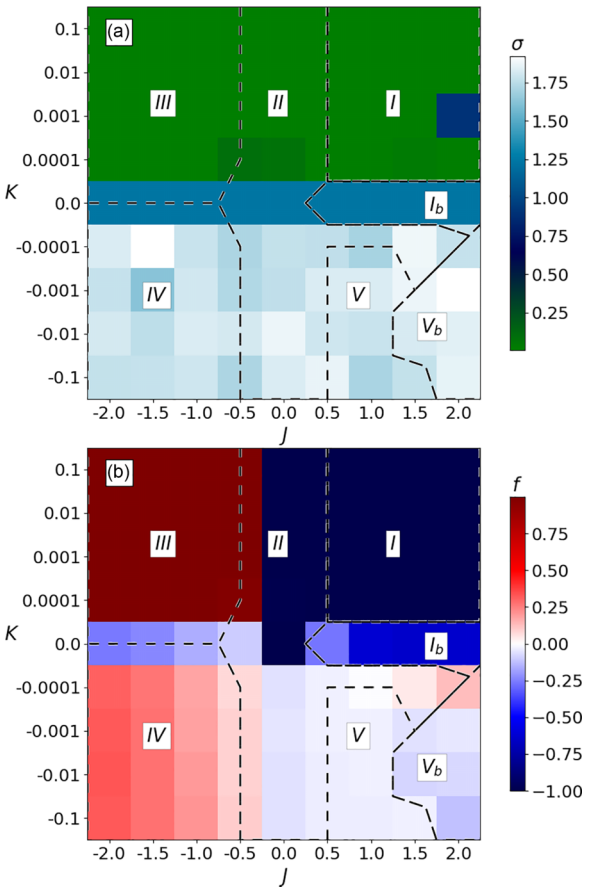

FIG. 6. (a) Standard deviation σ of the circularly averaged phase $\bar{\phi}$ of the disks. (b) The average frustration f in a system with $\rho = 0.49$ and $\tau = 1.5 \times 10^5$.

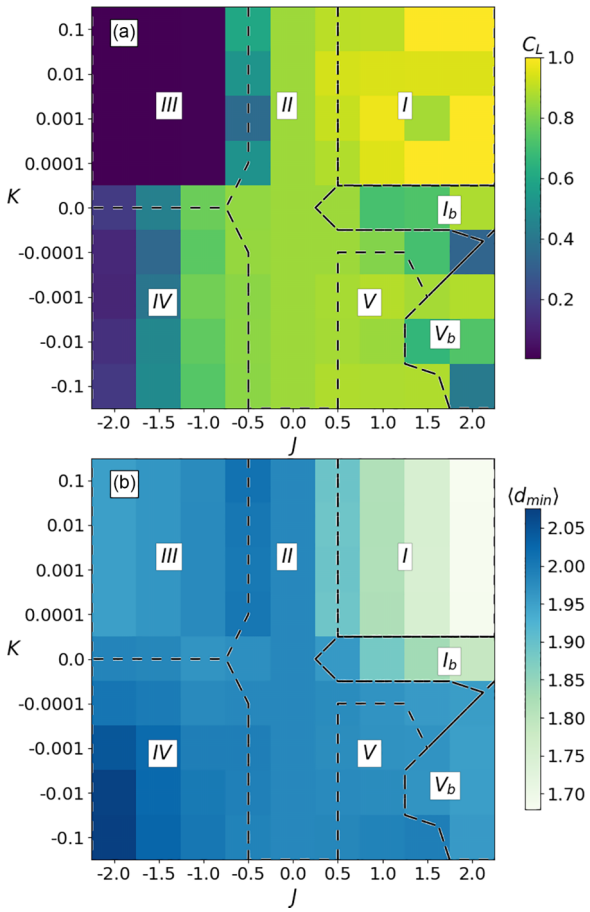

FIG. 7. (a) Fraction C_L of disks contained in the largest cluster present in the system. (b) The average shortest distance $\langle d_{\min} \rangle$ between neighboring disks in a system with $\rho = 0.49$ and $\tau = 1.5 \times 10^5$.

or the superlattice MIPS state, the frustration is intermediate but positive. Generally, as f gets closer to $f = +1$, the motion in the system becomes more fluidlike.

The average fraction C_L of disks in the largest cluster is defined by identifying groups of disks that are all in steric contact with each other as members of a single cluster. This quantity is computed using an efficient neighbor lookup table method [53] and is then averaged over time. In Fig. 7(a) we plot a heat map of C_L as a function of K versus J. In the active gel region I, C_L is large, while in the active labyrinthine region III, C_L is low since the repulsive swarmalator forces break the labyrinth structures into small disjoint clusters. For the MIPS-like regions IV and V, there is a substantial amount of clustering but C_L is lower than its value in the standard MIPS region II. We observe reduced clustering in region V_b, and the value of C_L is one of the criteria that we use to distinguish region V_b from region V.

In systems where pattern formation is possible, the average distance to the closest neighbor $\langle d_{\min} \rangle$ can be used to identify signatures of different patterns [46]. The closest neighbor of disk i is at a distance $d^i_{\min} = \min\{r_{ij}\}$ and we obtain $\langle d_{\min} \rangle = \langle N^{-1} \sum_i^N d^i_{\min} \rangle$, where we sum the shortest distance to the nearest particle over all particles and then divide by N, the number of particles, and then we take this average over time. Figure 7(b) shows a heat map of $\langle d_{\min} \rangle$ plotted as a function of K versus J. In the active gel region I, $\langle d_{\min} \rangle$ is small since all of the disks are in one giant cluster and the swarmalator force acts as a surface tension that further compresses the disks. There is a linear dependence of $\langle d_{\min} \rangle$ on J in the active labyrinthine region III since the increasing repulsion slightly reduces the size of the small clusters that appear in the labyrinth formation. In the frustrated MIPS region IV, $\langle d_{\min} \rangle$ reaches its lowest value for large J and K where the stripe-ordered dense clusters illustrated in Fig. 4(a) coexist with the maximum amount of the low density state with correlated internal parameters shown in Fig. 4(c). We used the values of σ, f, C_L, and $\langle d_{\min} \rangle$ to construct the dynamic phase diagram plotted in Fig. 2.

We next consider the impact of changing the activity τ and the density ρ on the dynamical behavior. In general, the gel regions I and I_b persist down to the lowest values of τ, but the process of gel aggregation becomes slower as τ decreases. The active labyrinthine region III is not modified by changes in τ. We focus on the behavior of the MIPS states in Fig. 8, where we plot heat maps of C_L as a function of ρ versus τ. In the frustrated MIPS region IV, shown in Fig. 8(a) at $J = -2$ and $K = -0.001$, MIPS only occurs for the highest densities and activities, indicating that the frustration interferes with the emergence of the MIPS. For the standard MIPS region II with

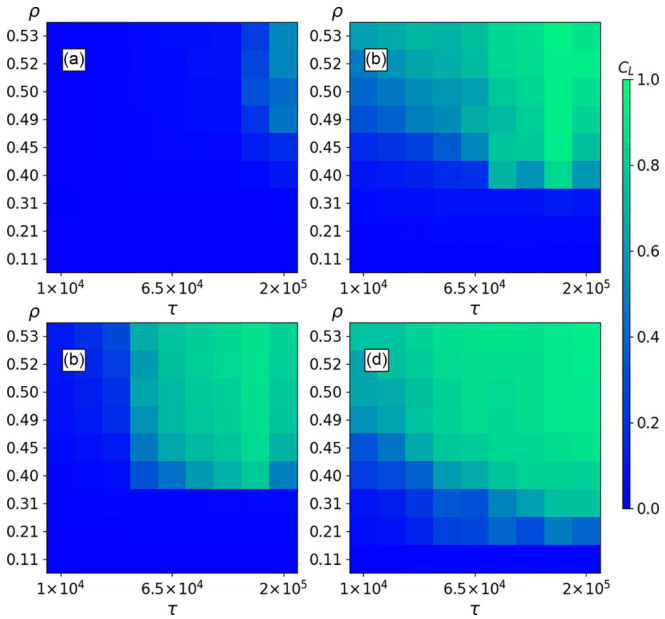

FIG. 8. The size of the largest cluster in the system, indicating the presence of MIPS when it encompasses the majority of the system (shaded green). (a) The frustrated MIPS region IV at $J = -2$ and $K = -0.001$. (b) The regular MIPS region II at $J = 0$ and $K = 0$. (c) The superlattice MIPS region V at $J = 1$ and $K = -0.01$. (d) The frustrated cluster fluid region V_b at $J = 2$ and $K = -0.001$.

$J = 0$ and $K = 0$, plotted in Fig. 8(b), MIPS extends down to a minimum density of $\rho = 0.4$ and a minimum run time of $\tau = 5 \times 10^4$, spanning a much larger window of ρ and τ than the frustrated MIPS region IV. MIPS is enhanced for the superlattice MIPS region V in Fig. 8(c), where $J = 1$ and $K = -0.01$. The superlattice ordering illustrated in Fig. 4(b) stabilizes the MIPS clusters and allows them to persist down to lower values of τ. The greatest enhancement of C_L occurs in region V_b, shown in Fig. 8(d) at $J = 2$ and $K = -0.001$. For these parameters, the system is not far from the arrested gel region I_b and the regular MIPS region II. Although the long range crystalline ordering of the superlattice found in the superlattice MIPS region V is absent, there is a longer range correlation of the values of ϕ_i within the clustered areas, as illustrated in Fig. 5(d). Neighboring disks have different internal parameters ϕ_i, but next-neighbor disks at a distance $r_{ij} = 4R_d$ have matching values of ϕ_i and tend to stabilize the cluster. This allows the disks in the gas phase to adhere more readily to the surface of the largest cluster since it is not necessary for them to attach at the precise location that would be required if long range ordering were present. As a result, the window of large C_L is maximized for the frustrated cluster fluid region V_b.

IV. DISCUSSION AND SUMMARY

Our active matter swarmalator model demonstrates that ordinary MIPS can be considered as a special case of a larger class of possible active phase separating behaviors. The internal parameter degree of freedom of each disk couples to the swarmalator rules and produces additional repulsive and attractive interactions between disks that can compete with or facilitate MIPS formation. The swarmalator model generates a wide variety of active phases, including an aggregating gel where activity speeds up aggregation, a phase arrested active gel, regular MIPS, frustrated MIPS with stripe phase ordering, a superlattice phase ordered MIPS, and several correlated active fluids with local internal parameter ordering. Future investigations could address whether there are additional dynamics within the solids with ordered internal parameters, such as periodic oscillations or propagating waves in which these parameters change. Additional dynamic behaviors could arise if a periodic external driving force were coupled to the internal internal parameter of the disks. Previously considered modifications to generic swarmalator models, such as temperature [54,55] or chirality [56], could also be introduced to the active disk system. In addition, instead of a continuously variable internal parameter, the internal parameter could be limited to discrete values in order to draw parallels with Ising or other spin systems. Our results are relevant to active colloidal systems with competing interactions, biological systems with particle-specific interactions, and robotic swarms. This work provides a model for interactions between frustrated systems and the MIPS state, and shows that in some cases, the frustration works against formation of MIPS, but under other conditions, the frustration can instead enhance MIPS.

ACKNOWLEDGMENTS

This work was supported by the US Department of Energy through the Los Alamos National Laboratory. Los Alamos National Laboratory is operated by Triad National Security, LLC, for the National Nuclear Security Administration of the U.S. Department of Energy (Contract No. 892333218NCA000001). A.L. was supported by a grant of the Romanian Ministry of Education and Research, CNCS - UEFISCDI, Project No. PN-III-P4-ID-PCE-2020-1301, within PNCDI III.

[1] M. C. Marchetti, J. F. Joanny, S. Ramaswamy, T. B. Liverpool, J. Prost, M. Rao, and R. A. Simha, Hydrodynamics of soft active matter, Rev. Mod. Phys. **85**, 1143 (2013).

[2] C. Bechinger, R. Di Leonardo, H. Löwen, C. Reichhardt, G. Volpe, and G. Volpe, Active particles in complex and crowded environments, Rev. Mod. Phys. **88**, 045006 (2016).

[3] G. Gompper, R. G. Winkler, T. Speck, A. Solon, C. Nardini, F. Peruani, H. Löwen, R. Golestanian, U. B. Kaupp, L. Alvarez, T. Kiørboe, E. Lauga, W. C. K. Poon, A. DeSimone, S. Muiños-Landin, A. Fischer, N. A. Söker, F. Cichos, R. Kapral, P. Gaspard *et al.*, The 2020 motile active matter roadmap, J. Phys.: Condens. Matter **32**, 193001 (2020).

[4] E. Lauga and T. R. Powers, The hydrodynamics of swimming microorganisms, Rep. Prog. Phys. **72**, 096601 (2009).

[5] R. Di Leonardo, L. Angelani, D. Dell'Arciprete, G. Ruocco, V. Iebba, S. Schippa, M. P. Conte, F. Mecarini, F. De Angelis, and

E. Di Fabrizio, Bacterial ratchet motors, Proc. Natl. Acad. Sci. USA **107**, 9541 (2010).
[6] T. Bhattacharjee and S. S. Datta, Confinement and activity regulate bacterial motion in porous media, Soft Matter **15**, 9920 (2019).
[7] T. H. Tan, A. Mietke, J. Li, Y. Chen, H. Higinbotham, P. J. Foster, S. Gokhale, J. Dunkel. and N. Fakhri, Odd dynamics of living chiral crystals, Nature (London) **607**, 287 (2022).
[8] O. Hallatschek, S. S. Datta, K. Drescher, J. Dunkel, J. Elgeti, B. Waclaw, and N. S. Wingreen, Proliferating active matter, Nat. Rev. Phys. **5**, 407 (2023).
[9] D. Helbing, Traffic and related self-driven many-particle systems, Rev. Mod. Phys. **73**, 1067 (2001).
[10] C. Castellano, S. Fortunato, and V. Loreto, Statistical physics of social dynamics, Rev. Mod. Phys. **81**, 591 (2009).
[11] M. J. Bowick, N. Fakhri, M. C. Marchetti, and S. Ramaswamy, Symmetry, thermodynamics, and topology in active matter, Phys. Rev. X **12**, 010501 (2022).
[12] S. Shankar, A. Souslov, M. J. Bowick, M. C. Marchetti, and V. Vitelli, Topological active matter, Nat. Rev. Phys. **4**, 380 (2022).
[13] M. Rubenstein, A. Cornejo, and R. Nagpal, Programmable self-assembly in a thousand-robot swarm, Science **345**, 795 (2014).
[14] G. Wang, T. V. Phan, S. Li, M. Wombacher, J. Qu, Y. Peng, G. Chen, D. I. Goldman, S. A. Levin, R. H. Austin, and L. Liu, Emergent field-driven robot swarm states, Phys. Rev. Lett. **126**, 108002 (2021).
[15] M. Y. B. Zion, J. Fersula, N. Bredeche, and O. Dauchot, Morphological computation and decentralized learning in a swarm of sterically interacting robots, Sci. Robot. **8**, eabo6140 (2023).
[16] M. Shaebani, A. Wysocki, R. Winkler, G. Gompper, and H. Rieger, Computational models for active matter, Nat. Rev. Phys. **2**, 181 (2020).
[17] P. Digregorio, D. Levis, A. Suma, L. F. Cugliandolo, G. Gonnella, and I. Pagonabarraga, Full phase diagram of active brownian disks: From melting to motility-induced phase separation, Phys. Rev. Lett. **121**, 098003 (2018).
[18] J. Stenhammar, D. Marenduzzo, R. Allena, and M. Catesa, Phase behaviour of active brownian particles: The role of dimensionality, Soft Matter **10**, 1489 (2014).
[19] M. Paoluzzi, D. Levis, and I. Pagonabarraga, From motility-induced phase-separation to glassiness in dense active matter, Commun. Phys. **5**, 111 (2022).
[20] Y. Fily and M. C. Marchetti, Athermal phase separation of self-propelled particles with no alignment, Phys. Rev. Lett. **108**, 235702 (2012).
[21] G. S. Redner, M. F. Hagan, and A. Baskaran, Structure and dynamics of a phase-separating active colloidal fluid, Phys. Rev. Lett. **110**, 055701 (2013).
[22] J. Palacci, S. Sacanna, A. P. Steinberg, D. J. Pine, and P. M. Chaikin, Living crystals of light-activated colloidal surfers, Science **339**, 936 (2013).
[23] I. Buttinoni, J. Bialké, F. Kümmel, H. Löwen, C. Bechinger, and T. Speck, Dynamical clustering and phase separation in suspensions of self-propelled colloidal particles, Phys. Rev. Lett. **110**, 238301 (2013).
[24] J. Bialké, J. T. Siebert, H. Löwen, and T. Speck, Negative interfacial tension in phase-separated active Brownian particles, Phys. Rev. Lett. **115**, 098301 (2015).
[25] M. E. Cates and J. Tailleur, Motility-induced phase separation, Annu. Rev. Condens. Matter Phys. **6**, 219 (2015).
[26] F. Ginot, I. Theurkauff, F. Detcheverry, C. Ybert, and C. Cottin-Bizonne, Aggregation-fragmentation and individual dynamics of active clusters, Nat. Commun. **9**, 696 (2018).
[27] A. K. Omar, H. Row, S. A. Mallory, and J. F. Brady, Mechanical theory of nonequilibrium coexistence and motility-induced phase separation, Proc. Natl. Acad. Sci. USA **120**, e2219900120 (2023).
[28] M. Seul and D. Andelman, Domain shapes and patterns - the phenomenology of modulated phases, Science **267**, 476 (1995).
[29] G. Malescio and G. Pellicane, Stripe phases from isotropic repulsive interactions, Nat. Mater. **2**, 97 (2003).
[30] M. A. Glaser, G. M. Grason, R. D. Kamien, A. Kosmrlj, C. D. Santangelo, and P. Ziherl, Soft spheres make more mesophases, Europhys. Lett. **78**, 46004 (2007).
[31] Q. Chen, S. C. Bae, and S. Granick, Directed self-assembly of a colloidal kagome lattice, Nature (London) **469**, 381 (2011).
[32] K. S. Khalil, A. Sagastegui, Y. Li, M. A. Tahir, J. E. Socolar, B. J. Wiley, and B. B. Yellen, Binary colloidal structures assembled through Ising interactions, Nat. Commun. **3**, 794 (2012).
[33] Y. Wang, Y. Wang, D. R. Breed, V. N. Manoharan, L. Feng, A. D. Hollingsworth, M. Weck, and D. J. Pine, Colloids with valence and specific directional bonding, Nature (London) **491**, 51 (2012).
[34] L. Pauling, The structure and entropy of ice and of other crystals with some randomness of atomic arrangement, J. Am. Chem. Soc. **57**, 2680 (1935).
[35] Y. Han, Y. Shokef, A. M. Alsayed, P. Yunker, T. C. Lubensky, and A. G. Yodh, Geometric frustration in buckled colloidal monolayers, Nature (London) **456**, 898 (2008).
[36] A. Ortiz-Ambriz and P. Tierno, Engineering of frustration in colloidal artificial ices realized on microfeatured grooved lattices, Nat. Commun. **7**, 10575 (2016).
[37] A. P. Ramirez, Geometric frustration: Magic moments, Nature (London) **421**, 483 (2003).
[38] C. Nisoli, R. Moessner, and P. Schiffer, Colloquium: Artificial spin ice: Designing and imaging magnetic frustration, Rev. Mod. Phys. **85**, 1473 (2013).
[39] S. H. Skjærvø, C. H. Marrows, R. L. Stamps, and L. J. Heyderman, Advances in artificial spin ice, Nat. Rev. Phys. **2**, 13 (2020).
[40] X. Guo, M. Guzmán, D. Carpentier, D. Bartolo, and C. Coulais, Non-orientable order and non-commutative response in frustrated metamaterials, Nature (London) **618**, 506 (2023).
[41] K. P. O'Keeffe, H. Hong, and S. H. Strogatz, Oscillators that sync and swarm, Nat. Commun. **8**, 1504 (2017).
[42] A. Barciś, M. Barciś, and C. Bettstetter, Robots that sync and swarm: A proof of concept in ROS 2, in *2019 International Symposium on Multi-Robot and Multi-Agent Systems (MRS)* (2019), pp. 98–104.
[43] S. Ceron, G. Gardi, K. Petersen, and M. Sitti, Programmable self-organization of heterogeneous microrobot collectives, Proc. Natl. Acad. Sci. USA **120**, e2221913120 (2023).
[44] Y. Jiao, T. Lau, H. Hatzikirou, M. Meyer-Hermann, J. C. Corbo, and S. Torquato, Avian photoreceptor patterns represent a disordered hyperuniform solution to a multiscale packing problem, Phys. Rev. E **89**, 022721 (2014).
[45] E. A. Jagla, Phase behavior of a system of particles with core collapse, Phys. Rev. E **58**, 1478 (1998).

[46] C. J. O. Reichhardt, C. Reichhardt, and A. R. Bishop, Structural transitions, melting, and intermediate phases for stripe- and clump-forming systems, Phys. Rev. E **82**, 041502 (2010).

[47] E. Pinçe, S. K. P. Velu, A. Callegari, P. Elahi, S. Gigan, G. Volpe, and G. Volpe, Disorder-mediated crowd control in an active matter system, Nat. Commun. **7**, 10907 (2016).

[48] F. A. Lavergne, H. Wendehenne, T. Baeuerle, and C. Bechinger, Group formation and cohesion of active particles with visual perception-dependent motility, Science **364**, 70 (2019).

[49] T. Bäuerle, R. C. Löffler, and C. Bechinger, Formation of stable and responsive collective states in suspensions of active colloids, Nat. Commun. **11**, 2547 (2020).

[50] See Supplemental Material at http://link.aps.org/supplemental/10.1103/PhysRevE.109.024607 for videos of the phases mentioned in Fig. 3.

[51] Y. Shokef and T. C. Lubensky, Stripes, zigzags, and slow dynamics in buckled hard spheres, Phys. Rev. Lett. **102**, 048303 (2009).

[52] A. Hill, M. Tanaka, K. B. Aptowicz, C. K. Mishra, A. G. Yodh, and X. Ma, Depletion-driven antiferromagnetic, paramagnetic, and ferromagnetic behavior in quasi-two-dimensional buckled colloidal solids, J. Chem. Phys. **158**, 194903 (2023).

[53] S. Luding and H. J. Herrmann, Cluster-growth in freely cooling granular media, Chaos **9**, 673 (1999).

[54] G. K. Sar and D. Gosh, Dynamics of swarmalators: A pedagogical review, Europhys. Lett. **139**, 53001 (2022).

[55] H. Hong, K. P. O'Keeffe, J. S. Lee, and H. Park, Swarmalators with thermal noise, Phys. Rev. Res. **5**, 023105 (2023).

[56] S. Ceron, K. O'Keeffe, and K. Petersen, Diverse behaviors in non-uniform chiral and non-chiral swarmalators, Nat. Commun. **14**, 940 (2023).